Role of protein dynamics in ion selectivity and allosteric coupling in the NaK channel

Joshua B. Brettmann[a], Darya Urusova[b], Marco Tonelli[c], Jonathan R. Silva[b], and Katherine A. Henzler-Wildman[a,c,1]

[a]Department of Biochemistry and Molecular Biophysics, Washington University School of Medicine, St. Louis, MO 63110; [b]Department of Biomedical Engineering, Washington University in Saint Louis, St. Louis, MO 63130; and [c]Department of Biochemistry, University of Wisconsin–Madison, Madison, WI 53706

Edited by Richard W. Aldrich, The University of Texas at Austin, Austin, TX, and approved November 9, 2015 (received for review August 12, 2015)

Flux-dependent inactivation that arises from functional coupling between the inner gate and the selectivity filter is widespread in ion channels. The structural basis of this coupling has only been well characterized in KcsA. Here we present NMR data demonstrating structural and dynamic coupling between the selectivity filter and intracellular constriction point in the bacterial nonselective cation channel, NaK. This transmembrane allosteric communication must be structurally different from KcsA because the NaK selectivity filter does not collapse under low-cation conditions. Comparison of NMR spectra of the nonselective NaK and potassium-selective NaK2K indicates that the number of ion binding sites in the selectivity filter shifts the equilibrium distribution of structural states throughout the channel. This finding was unexpected given the nearly identical crystal structure of NaK and NaK2K outside the immediate vicinity of the selectivity filter. Our results highlight the tight structural and dynamic coupling between the selectivity filter and the channel scaffold, which has significant implications for channel function. NaK offers a distinct model to study the physiologically essential connection between ion conduction and channel gating.

solution NMR | ion channels | membrane protein | protein dynamics

Ion conduction through the pore domain of cation channels is regulated by two gates: an inner gate at the bundle crossing of the pore-lining transmembrane helices and an outer gate located at the selectivity filter (Fig. 1 *B* and *C*). These two gates are functionally coupled as demonstrated by C-type inactivation, in which channel opening triggers loss of conduction at the selectivity filter (1–4). A structural model for C-type inactivation has been developed for KcsA, with selectivity filter collapse occurring upon channel opening (4–10). In the reverse pathway, inactivation of the selectivity filter has been linked to changes at the inner gate (5–14). However, flux-dependent inactivation occurs in Na^+ and Ca^{2+} channels as well and would likely require a structurally different mechanism to explain coupling between the selectivity filter and inner gate (7, 13–18).

This study provides experimental evidence of structural and dynamic coupling between the inner gate and selectivity filter in the NaK channel, a nonselective cation channel from *Bacillus cereus* (19). These results were entirely unexpected given the available high-resolution crystal structures (20, 21). The NaK channel has the same basic pore architecture as K^+ channels (Fig. 1 *B* and *C*) and has become a second model system for investigating ion selectivity and gating due to its distinct selectivity filter sequence ($_{63}$TVGDGN$_{68}$) and structure (19–23). Most strikingly, there are only two ion binding sites in the selectivity filter of the nonselective NaK channel (Fig. 1*A*) (21, 24). However, mutation of two residues in the selectivity filter sequence converts the NaK selectivity filter to the canonical KcsA sequence ($_{63}$TVGYGD$_{68}$; Fig. 1 *A* and *B*), leading to K^+ selectivity and a KcsA-like selectivity filter structure with four ion binding sites (21, 23). This K^+-selective mutant of NaK is called NaK2K. Outside of the immediate vicinity of the two mutations in the selectivity filter, high-resolution crystal structures of NaK and NaK2K are essentially identical (Fig. 1*B*) with an all-atom rmsd of only 0.24 Å.

NaK offers a distinct model to study the physiologically essential connection between ion conduction and channel gating because there is no evidence for any collapse or structural change in the selectivity filter. The NaK selectivity filter structure is identical in Na^+ or K^+ (22) and even in low-ion conditions (25), consistent with its nonselective behavior. Even the selective NaK2K filter appears structurally stable in all available crystal structures (25). Here we use NMR spectroscopy to study bicelle-solubilized NaK. Surprisingly, we find significant differences in the NMR spectra of NaK and NaK2K that extend throughout the protein and are not localized to the selectivity filter region. This, combined with NMR dynamics studies of NaK, suggests a dynamic pathway for transmembrane coupling between the inner gate and selectivity filter of NaK.

Results

NaK Is Functionally Reconstituted in Isotropic Bicelles and Is Suitable for Solution NMR. NaK is small and highly stable, facilitating high-resolution NMR studies. We first performed radioactive rubidium flux assays to confirm that NaK produced in our laboratory and reconstituted into proteoliposomes was functional (26) (Fig. S1). For NMR, NaK proteoliposomes were solubilized with DHPC to create lipid bicelles, as described in our previously published protocol (27).

The 2D-TROSY HSQC spectra of NaK in bicelles provide insight into both the structure and the dynamics of the protein. These spectra are of the NaKΔ19 construct with the M0 helix truncated, which is referred to as NaK throughout. Information is contained in both the observed chemical shifts and the peak dispersion, as well as the number of peaks and their relative intensities. The spectrum of NaK solubilized in $q = 0.33$ DMPC:

Significance

Pore domains of ion channels form the ion conduction pathway and thus control the identity and flux of ions across the membrane. Flux-dependent inactivation suggests that these two functions are connected, with allosteric linkage between the selectivity filter and inner gate. This study uses solution NMR to investigate structural and dynamic features of ion selectivity and coupling between the gates in the small bacterial channel NaK. NaK is a nonselective cation channel and is homologous to several eukaryotic channels that are not well modeled by KcsA. Our results show a previously unexpected dynamic coupling between the selectivity filter and inner gate in NaK. This suggests that such transmembrane communication is widespread and occurs through distinct mechanisms in diverse channels.

Author contributions: J.B.B., J.R.S., and K.A.H.-W. designed research; J.B.B., D.U., and M.T. performed research; J.B.B. and K.A.H.-W. analyzed data; and J.B.B. and K.A.H.-W. wrote the paper.

The authors declare no conflict of interest.

This article is a PNAS Direct Submission.

Data deposition: NMR, atomic coordinates, chemical shifts, and restraints have been deposited in Biological Magnetic Resonance Data Bank (BMRB), www.bmrb.wisc.edu (accession no. 26617).

[1]To whom correspondence should be addressed. Email: henzlerwildm@wisc.edu.

This article contains supporting information online at www.pnas.org/lookup/suppl/doi:10.1073/pnas.1515965112/-/DCSupplemental.

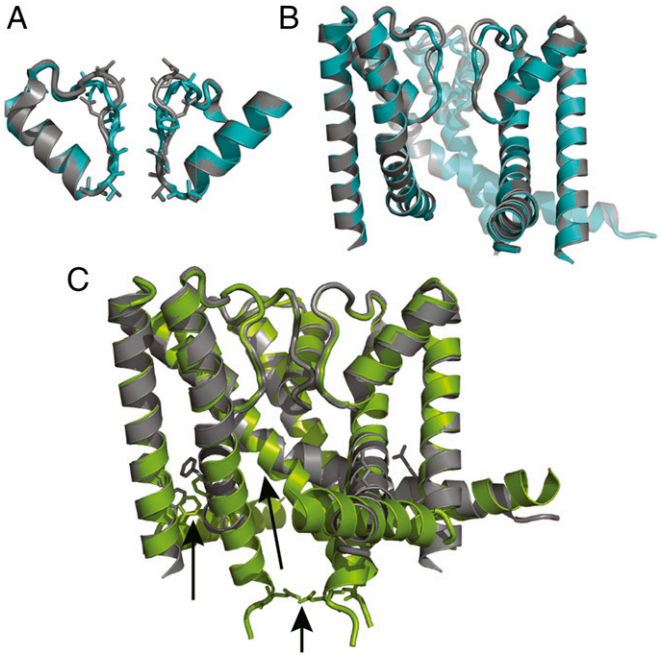

Fig. 1. Crystal structures of the nonselective cation channel NaK and the potassium-selective NaK2K mutant show structural changes restricted to the area of the selectivity filter. Alignment of the WT NaK (gray; PDB 3E8H) and NaK2K (light blue; PDB 3OUF) selectivity filters shows a KcsA-like four-ion-binding-site selectivity filter is created by the NaK2K mutations (D66Y and N68D) (*A*), but no structural changes occur outside the vicinity of the selectivity filter (*B*). (*C*) Full-length NaK (green; PDB 2AHZ) represents a closed conformation. Alignment of this structure with NaK (gray) highlights the changes in the M2 hinge (arrow), hydrophobic cluster (residues F24, F28, and F94 shown as sticks), and constriction point (arrow; residue Q103 shown as sticks) upon channel opening. Two (*A*) or three monomers (*B* and *C*) from the tetramer are shown for clarity.

DHPC bicelles at 45 °C displays excellent peak dispersion (Fig. 2), indicating that NaK is well folded under these conditions. Helical membrane proteins often have significant peak overlap due to the modest dispersion of amide chemical shifts in helical regions and the uniformity of the membrane environment. The good dispersion observed for NaK suggests that the helices are tightly packed with a well-defined tertiary structure resulting in unique chemical shifts. Eighty-three percent of NaK peaks have been assigned at 65 °C (Figs. S2 and S3), and the secondary structure of NaK determined from the chemical shift index matches the crystal structure (PDB 3E8H) quite well (Fig. 2, *Inset*) (28, 29). These spectra confirm the structural stability of NaK in isotropic bicelles up to 65 °C, as expected from its thermal stability, and establish the suitability of these conditions for detailed investigation of channel structure and dynamics by solution NMR.

Nonselective NaK and Selective NaK2K Have Extensive Chemical Shift Differences. Our initial goal was to compare the backbone dynamics of NaK and NaK2K to experimentally test the role of dynamics in ion selectivity. However, ^{1}H-^{15}N TROSY-HSQC spectra of NaK2K revealed widespread chemical shift differences (Fig. 3) that were completely unexpected on the basis of the available crystal structures. In the high-resolution crystal structures of NaK and NaK2K, differences are highly localized to the selectivity filter region only (Fig. 1*B*) (21). We therefore expected relatively few peak shifts when comparing spectra of NaK and NaK2K bound to K^{+}, localized to the region in and around the selectivity filter. Instead, we observed widespread chemical shift changes (Fig. 3). The major difference between crystallography and NMR is that a single structural state of a protein is trapped within a crystal, whereas the NMR data represent the population-weighted average of all states present in the bicelle. Thus, these chemical shift differences may be explained by a shift in protein structure between NaK and NaK2K that is not captured in the crystal, or they could arise from changes in the equilibrium distribution of states sampled by NaK and NaK2K. Due to these significant chemical shift differences, NaK2K was independently assigned. Each of the individual point mutations (D66Y or N68D) has a spectrum with only minor chemical shift differences compared with NaK (Fig. S4).

Mapping the chemical shift changes between NaK and NaK2K onto the NaK structure shows the largest differences are in the selectivity filter region as expected (Fig. 3*B*). Significant chemical shift differences are also seen in the M2 helix in regions that change conformation upon channel opening/closing. This includes the hinge region, which bends upon opening/closing of the inner gate (residues G87 and G89), a hydrophobic patch that rearranges upon channel opening (F94 and I95) and the constriction point

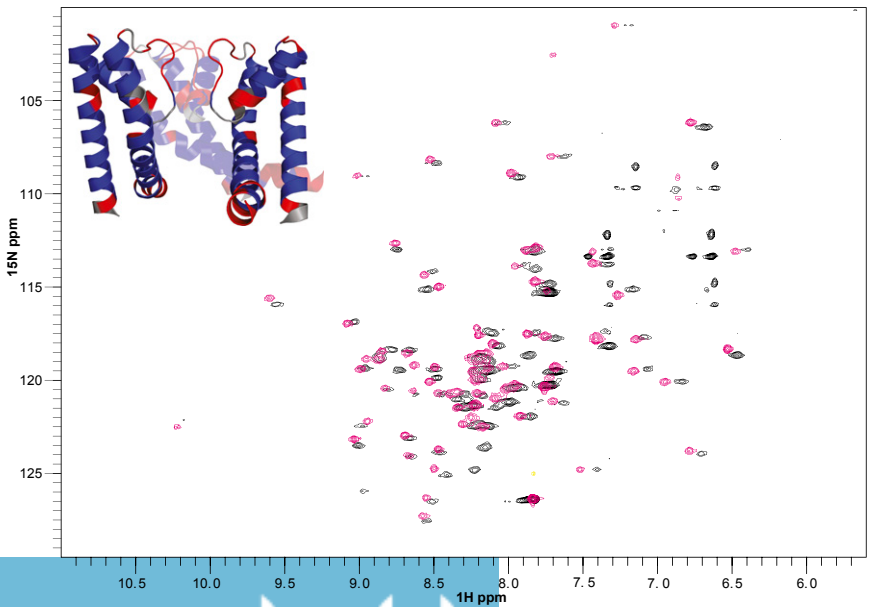

Fig. 2. The ^{15}*N*-TROSY HSQC NMR spectra of NaK in isotropic bicelles reflect a stable, well-folded protein. Spectra of NaK in 3:1 DHPC:DMPC isotropic bicelles at 45 °C (black) and 65 °C (magenta) show only minor chemical shift changes, reflecting the high thermal stability of NaK. *Inset* shows the secondary structure predicted from the backbone chemical shift index using TALOS+ (29) mapped onto the NaK crystal structure (PDB 3E8H) with alpha helical regions colored blue, loops red, and unassigned residues gray. Three monomers of the channel are shown for clarity.

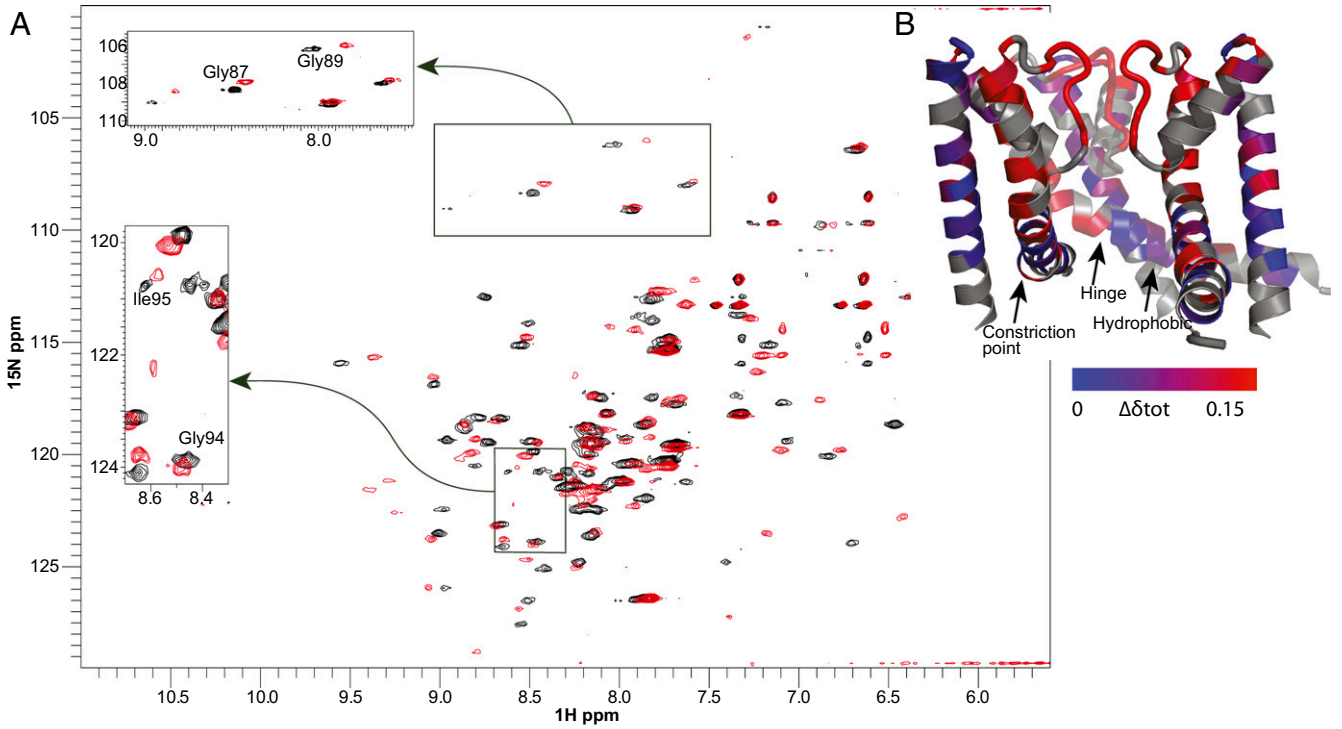

Fig. 3. NMR spectra reveal differences between NaK and NaK2K are not localized to the selectivity filter but extend throughout the channel. (*A*) Comparing ^{15}N TROSY-HSQC spectra of NaK (black) and NaK2K (red) reveals widespread amide chemical shift changes. These differences occur for many more residues than would be expected based on the crystal structures (Fig. 1). *Insets* highlight residues in the M2 helix far from the selectivity filter mutations that create NaK2K. (*B*) The chemical shift differences between NaK and NaK2K are plotted on the NaK structure (PDB 3E8H) with a blue to red color scale. This highlights the significant chemical shift changes that extend throughout the M2 helix, including the hinge region and hydrophobic patch near the intracellular constriction point (arrows), regions where structural changes occur between the open and closed channel.

formed by the M2 helix (N101 and Q103) (Fig. 3 *A* and *B*, arrow) (20). Some of these residues are over 25 Å away from the site of mutation, well beyond the range of simple effects of mutation on neighboring residues or structural differences predicted by the crystal structures. This demonstrates that the sequence and structural state of the selectivity filter affects the entire NaK protein and is coupled to the inner gate.

Such coupling between the selectivity filter and the inner gate is well established in KcsA and several other K^+ channels but has not previously been demonstrated for NaK, which has a much more stable structural scaffold. This leads to a number of questions. (*i*) Are the chemical shift changes an artifact of experimental conditions? (*ii*) Is coupling between the gates inherent to NaK or introduced upon creation of a selective filter? (*iii*) Can coupling be observed due to changes at the inner gate?

Coupling Is Not an Artifact of Experimental Conditions. One striking difference between KcsA and NaK is the stability of the NaK selectivity filter in various ionic conditions. We therefore tested whether this was true in our NMR samples. Spectra of NaK in bicelles with K^+ only, Na^+ only, or low salt show very minor shifts that are localized to the selectivity filter and adjacent regions (Fig. S5). Residues D66, G67, and S70 are sensitive to ion identity, consistent with differences in ion binding at the top of the selectivity filter in the crystal structures (22). The NMR data are thus consistent with the lack of selectivity filter collapse observed crystallographically. This prominent feature of NaK makes it an interesting model system to compare with KcsA, where structural changes in the selectivity filter are integral to coupling between the gates.

The secondary structure determined from the chemical shift index is very similar between NaK and NaK2K and closely matches the crystal structures (Fig. S6) (29). Together, the secondary structure and ion binding data support the high stability and proper folding of NaK in bicelles. Then what can explain the observed chemical shift differences between NaK and NaK2K? Although the crystal structures represent a high-resolution snapshot of a single state, the single set of peaks observed in the NMR spectrum reflects the population-weighted average of all of the states sampled by NaK. A shift in the equilibrium distribution of structural states between NaK and NaK2K could lead to the observed chemical shift differences. To test this hypothesis, we further assessed the dynamics of NaK and NaK2K.

Coupling Between Gates Is Inherent to NaK. To determine if coupling between gates is an inherent property of the nonselective NaK channel, we measured NaK dynamics on the microsecond–millisecond timescale using ^{15}N-TROSY-CPMG experiments (Fig. 4). Due to the inherent insensitivity of these experiments, full deuteration of the protein is required. This reduces the number of residues that can be monitored because of limited back exchange of amide protons in this highly stable channel. The figure shows ΔR_2 (Fig. 4), determined as described in *Methods*. CPMG experiments monitor the transverse relaxation rate (R_2), which includes intrinsic relaxation plus additional line broadening due to loss of coherence upon conformational exchange between states with different chemical shift values. The exchange contribution to the apparent R_2 can be suppressed by rapid pulsing during the CPMG experiment. By comparing CPMG experiments performed with slow (low ν_{CPMG}) and fast (high ν_{CPMG}) pulsing, intrinsic relaxation is eliminated and ΔR_2 reflects only the exchange contribution to the transverse relaxation rate. Thus, ΔR_2 will be 0 if there are no microsecond–millisecond timescale dynamics, and ΔR_2 will be positive if there is conformational exchange on this timescale. The results show conformational exchange throughout the protein, particularly at the bottom of the selectivity filter and the hinge point in M2, as well as at the constriction point on the intracellular side of the channel. Because CPMG experiments detect dynamics only when the exchanging states have different

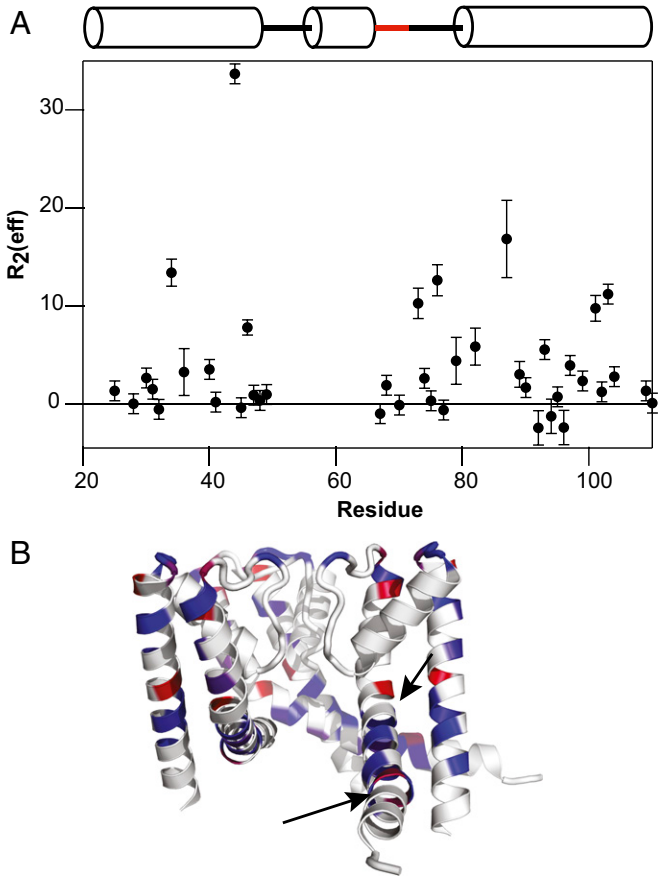

Fig. 4. Dynamics on the microsecond–millisecond timescale in NaK extend across the membrane. (*A*) ΔR_2 (s^{-1}) measured with a two-point TROSY-CPMG NMR experiment. Residues were excluded if they were too weak for quantitative analysis, unassigned or overlapped. The secondary structure is indicated at the top (selectivity filter in red). (*B*) ΔR_2 (s^{-1}) data shown on the NaK structure with a blue ($\Delta R_2 = 0$) to red (high ΔR_2) color scale. Dynamics on the microsecond–millisecond timescale are detected in the selectivity filter as well as the M2 hinge region and intracellular constriction point (arrows), regions where conformational change occurs upon channel opening/closing.

chemical shifts, not every residue in a region that is exchanging will have a measurable ΔR_2. The regions with the most significant ΔR_2 values are exactly where local structural changes occur between the open and closed channel (20) (Figs. 1*C* and 4). These results support the idea that transmembrane allostery between the selectivity filter and intracellular gate is an inherent property in NaK. Because there is no reason a priori to assume two-state exchange and the available electrophysiology data on NaK are not sufficient for quantitative comparison of rates and populations, we did not attempt further quantitative analysis of the exchange process.

Dynamic Shift Between NaK and NaK2K. Does the coupling observed upon mutation of NaK to NaK2K arise from changes in equilibrium dynamic state? To assess dynamic differences between NaK and NaK2K, peak intensities were compared between the two spectra. Increased protein motion leads to line-broadening and a decrease in peak intensity. For comparison, peak intensities were normalized to the C-terminal residue, N110, which is far from the site of mutation and has identical chemical shifts in NaK and NaK2K. This approach, rather than comparison of ΔR_2 values, was used because deuteration of NaK and NaK2K for CPMG experiments severely limits the number of residues that can be analyzed. Comparison of peak intensity provides data for more residues throughout the protein and is sensitive to dynamics on a broader range of timescales, including faster fluctuations of the amide bond vector. NaK2K has stronger peak intensities in the region around the selectivity filter, particularly for residues in the pore helix (I51 and L54), but also in the surrounding loops (Fig. 5). Outside this scaffold region, differences in peak intensity between NaK and NaK2K are less significant, with an increase in peak intensity for NaK at the constriction point. This suggests that the scaffold behind the K^+-selective NaK2K selectivity filter is less dynamic or more structurally homogenous than in nonselective NaK. These results are consistent with a role for structural stability in maintaining a four-site ion-selective filter and K^+-selectivity, a phenomenon that has been extensively studied previously (30). They also suggest that the observed coupling between the gates is tuned by the dynamic state of the protein.

Changing State of the Inner Gate Leads to Changes Above the Hinge. One convincing way to demonstrate coupling between the inner gate and selectivity filter is to show that this coupling works both ways. To test this, we recorded spectra of full length NaK including the M0 helix (identified throughout as FLNaK). FLNaK provides a good model of the closed state based on both the crystal structure and ion flux assays (Fig. 1*C*) (19). Initial assessment of this spectrum reveals peak doubling, which reveals that FLNaK exists in two states in isotropic bicelles at 45 °C (Fig. 6 and Fig. S7). Upon raising the temperature to 65 °C, each pair of peaks merges to a single peak, demonstrating that these two states are able to interconvert (Fig. S8). Examining only well-resolved and assigned residues reveals this peak doubling occurs throughout the protein with similar populations of the two states. This suggests a global two-state exchange process, although the states cannot be assigned from these data alone (Fig. 6). Further, chemical shift differences between NaK (open-state model) and FLNaK (closed state model) extend above the hinge on the M2 helix (Fig. S9), demonstrating reverse coupling from the inner gate to the scaffold directly behind the selectivity filter.

Discussion

Implications for Ion Selectivity. The structural stability of NaK has enabled engineering of the selectivity filter, tuning the number of ion binding sites and ion selectivity of the channel (21, 23). Beautiful high-resolution crystal structures of these different mutants have contributed to our current understanding of the structure–function relationships underlying ion selectivity and support the model that four ion binding sites are necessary for potassium selectivity through a knock-on mechanism (21–23, 25, 31–33). Here we present NMR data on the NaK channel solubilized in isotropic bicelles, adding experimental insight into the dynamics of the protein.

The scaffold holding the selectivity filter has long been appreciated for its important role in tuning selectivity in K^+ channels (7, 13). Our results extend this idea in the NaK channel by revealing increased rigidity of the scaffold when the selectivity filter is K^+-selective and less rigidity of the scaffold when the selectivity filter is nonselective (Fig. 5*B*). This complements NMR studies of KcsA that show line broadening in the selectivity filter and scaffold for a mutation that decreases selectivity (12). Our data suggest that a more rigid scaffold may be necessary to stabilize a selectivity filter structure with four ion binding sites, and K^+-selectivity is thought to require four ion binding sites (24, 34).

Transmembrane Coupling in NaK. Coupling between gates has been well established for a number of ion channels; however, the mechanistic conservation of this coupling has not been studied. Our solution NMR provides initial experimental insight into the motion of the NaK channel. FLNaK, which crystallized in the closed form, displays clear peak doubling throughout the spectra (19). This is indicative of two states that interconvert slowly (millisecond–second timescale) (Fig. 6). Removal of the M0 helix creates the NaK construct, which crystallized in the open state. The NMR experiments reveal that NaK is still undergoing

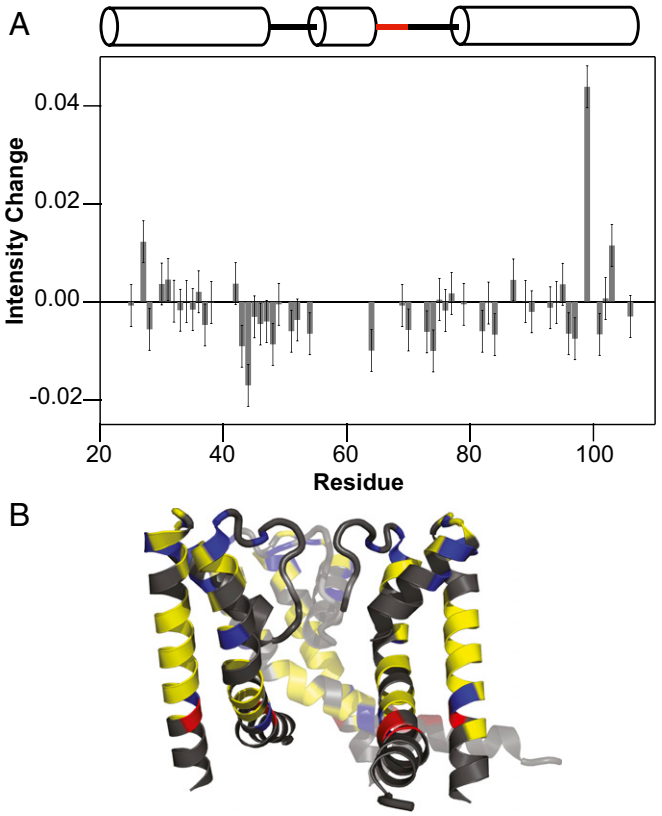

Fig. 5. Changes in peak intensity between NaK and NaK2K reflect dynamic differences in the scaffold behind the selectivity filter. (*A*) Plot of the difference in peak intensities between NaK and NaK2K. Positive values indicate more intense peaks in NaK. Peaks that are unassigned, overlapped, or within 5 Å of mutation sites were excluded from analysis. Secondary structure is indicated at the top (selectivity filter in red). (*B*) Residues with more intense peaks in NaK2K are mapped onto the crystal structure (PDB 3E8H) in blue, and residues with more intense peaks in NaK are shown in red. Residues with no significant change are colored yellow, and residues that are unassigned, overlapped, or very close to the points of mutation are gray. More intense peaks in NaK2K are consistent with a more rigid scaffold supporting the selectivity filter in this mutant.

conformational exchange, just on a faster microsecond–millisecond timescale. These dynamics occur throughout the M2 helix, including the hinge and channel constriction point, providing a dynamic pathway connecting the selectivity filter to the inner channel gate (Figs. 3*B* and 4*B*). Motion on this timescale is often correlated with exchange between functional states in the case of enzymes (35). Although we cannot currently assign the conformational exchange process to functional states of the channel, we note that the residues sensing motion are localized to the regions of NaK that would change environment upon channel opening/closing.

Coupling between gates occurs in both directions, as changes in the selectivity filter lead to significant changes at the inner gate as shown by the NaK2K mutation (Fig. 3*B*). The regions with microsecond–millisecond dynamics in NaK are the same regions with the largest chemical shift changes between NaK and NaK2K (Figs. 3*B* and 4*B*). This suggests that formation of a rigid K^+-selective filter leads to changes in the equilibrium state of the M2 hinge and the inner gate, a distant but functionally important site.

How does our observed coupling compare with KcsA? In KcsA, major structural rearrangements at the selectivity filter lead to its collapse and loss of ion conduction (3). This collapsed state is communicated to the inner gate by interactions with the scaffold (36), similar to our proposed path of communication between the gates in NaK. However, in NaK there is no evidence for collapse or even minor ion-dependent structural changes in the NaK selectivity filter by crystallography or NMR (Fig. S5). Thus, the dynamic coupling between the gates in NaK must work through a different mechanism. NaK is a flickery channel, and flicker gating has been suggested to arise from changes in conduction at the selectivity filter (21). However, NaK electrophysiology is limited, and the current structural data do not provide any insight into how the rigid NaK selectivity filter could cause changes in ion conduction. Thorough single channel recordings of this system combined with more quantitative NMR studies will be needed to resolve the role of the selectivity filter in channel gating and the mechanism linking the selectivity filter to the inner gate.

Our results emphasize the intimate connections between the selectivity filter and the overall channel structure. These interactions are important for both structural stability of the selectivity filter and dynamic coupling between the filter and inner channel gate, which will determine overall flux through the ion channel.

Methods

Expression and Purification of NaK. NaK constructs were missing the first 19 amino acids, corresponding to the NaKΔ19 construct used to determine most crystal structure of NaK and NaK mutants (21, 23). NaKΔ19 is referred to as NaK throughout to emphasize the different mutations within this construct that are the focus of this work. NaK and the mutants studied here were purified largely as published (20, 27), with a few changes to optimize expression in minimal media. NaK was transferred from NaK-pQE60 (generously provided by Youxing Jiang) to a pET15B vector with an N-terminal 6xHis tag. This led to 2–3× higher yield of NaK when expressed in minimal media for isotopic labeling. Expression of NaK is described in detail in *Supporting Information*. In brief, NaK was overexpressed in BL21 (DE3) cells in M9 minimal media and induced with IPTG (isopropyl-beta-D-thiogalactopyranoside) at 20 °C for 16–20 h. The membrane fraction was isolated and solubilized in 20 mM DM (n-decyl-beta-D-maltopyranoside). NaK was purified by IMAC (immobilized-metal affinity chromatography) with Talon cobalt affinity resin (Clontech) and size exclusion chromatography on a Superdex 200 column.

Reconstitution into Isotropic Bicelles. NaK concentration was determined by A280 using the calculated extinction coefficient of 3,840 $L \cdot mol^{-1} \cdot cm^{-1}$. NaK was reconstituted into bicelles using our previously published protocol with slight alterations (27). DMPC (1,2-dimyristoyl-*sn*-glycero-3-phosphocholine) was hydrated at 20 mg/mL in NMR buffer, bath sonicated ~1 min and solubilized with 10 mM DM for 20 min. NaK with the His-tag removed was added to the solubilized DMPC at a molar ratio of 1:100 NaK monomer/DMPC and rotated at room temperature for 3 h. Two aliquots of 45 mg Amberlite XAD-2 (BioRad) per milligram of total detergent were added to remove the detergent and incubated overnight at room temperature. Amberlite was removed, and the NaK proteoliposomes were ultracentrifuged at 150,000 × *g* for 2 h at 6 °C. The proteoliposome pellet was solubilized with DHPC (1,2-dihexanoyl-*sn*-glycero-3-phosphocholine) dissolved in NMR buffer to create

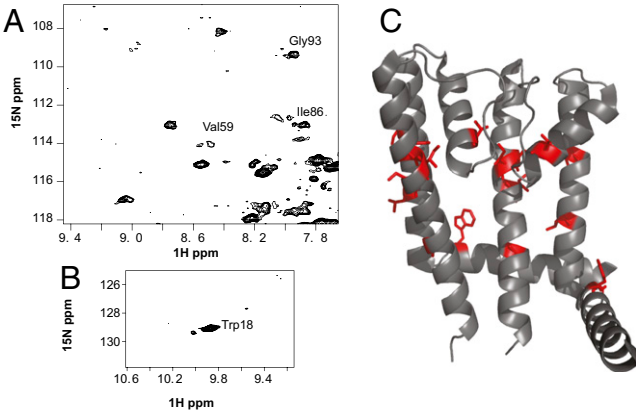

Fig. 6. Global exchange on a slow timescale in FLNaK. Peak doubling occurs for many residues in FLNaK at 45 °C (*A* and *B*) (the full spectrum is shown in Fig. S5), reflecting two states in slow (~50 s^{-1} or slower) exchange. (*C*) Well-resolved and assigned peaks with clear two-state exchange are shown on the FLNaK structure (PDB 2AHZ). All of these residues have similar populations for the two states, supporting a global exchange process.

q = 0.33 DMPC/DHPC bicelles. Four freeze–thaw cycles produced homogeneous bicelles containing NaK, which were flash-frozen and stored at –80 °C until use.

NMR Experiments. NMR samples contained 0.5–1.5 mM NaK in q = 0.33 DMPC/DHPC bicelles in 100 mM MOPS, 40 mM KCl, pH 7 with 10% D_2O. Samples with different salt conditions, as described in the text, were prepared using the desired final buffer/salt for the S200 column and all subsequent steps. The ^{1}H-^{15}N TROSY spectra were collected on a 700-MHz Varian spectrometer with a room temperature probe. Three-dimensional backbone walk experiments were acquired on a 600-MHz Bruker spectrometer with cryoprobe (Washington University) or 750-MHz Bruker spectrometer with cryoprobe [National Magnetic Resonance Facility at Madison (NMRFAM)]. TROSY-HNCA, BEST-TROSY HNCA, BEST-TROSY HN(co)CA, and BEST-TROSY HNCACB (37, 38) were collected using a nonuniform 10% poisson-gap sampling schedule (39), reconstructed using istHMS (40), processed using nmrpipe (41) and analyzed with CCPNMR Analysis (42). Backbone walk experiments were supplemented with 1–$^{13}C'$-amino acid specific labeling (43). Assignments were submitted to the Biological Magnetic Resonance Data Bank (BMRB).

Chemical shift differences ($\Delta\delta_{tot}$) were calculated using Eq. **1**,

$$\Delta\delta_{tot} = \sqrt{(\Delta\delta_H)^2 + (0.154\Delta\delta_N)^2}. \quad [1]$$

TROSY-CPMG (44, 45) experiments were performed on an 800-MHz Varian spectrometer with a cryoprobe (NMRFAM), with a relaxation delay (T_{relax}) of 40 ms. Two CPMG field strengths were acquired at ν_{CPMG} = 100 Hz and ν_{CPMG} = 1,000 Hz. $\Delta R_{2,app}$ was determined with Eq. **2**, with $I_{\nu CPMG}$ and I_0 being the peak intensities with and without CPMG refocusing periods. ΔR_2 was calculated for all well-resolved residues using Eqs. **2** and **3** (46):

$$R_{2,app} = -\frac{1}{T_{relax}} \times \ln\left[\frac{I(\nu_{CPMG})}{I_0}\right], \quad [2]$$

$$\Delta R_2 = R_{2,app}(\nu_{CPMG=100Hz}) - R_{2,app}(\nu_{CPMG=1,000Hz}). \quad [3]$$

ACKNOWLEDGMENTS. We thank Youxing Jiang for the original NaK-pQE60 plasmid. We thank Colin Nichols for assistance with radioactive rubidium flux assays. We thank Greg DeKoster and Chao Wu for assistance with NMR acquisition. This study made use of the National Magnetic Resonance Facility at Madison, which is supported by NIH Grant P41GM103399 [National Institutes of General Medical Sciences (NIGMS)]; old number: P41RR002301. Equipment was purchased with funds from the University of Wisconsin–Madison, the NIH (P41GM103399, S10RR02781, S10RR08438, S10RR023438, S10RR025062, and S10RR029220), the National Science Foundation (NSF) (DMB-8415048, OIA-9977486, and BIR-9214394), and the US Department of Agriculture (USDA). This work was supported by the Searle Scholars Program (K.A.H.-W.) and Burroughs Wellcome Fund Career Award at the Scientific Interface (1010299 to J.R.S.).

1. Chakrapani S, Cordero-Morales JF, Perozo E (2007) A quantitative description of KcsA gating I: Macroscopic currents. *J Gen Physiol* 130(5):465–478.
2. Chakrapani S, Cordero-Morales JF, Perozo E (2007) A quantitative description of KcsA gating II: Single-channel currents. *J Gen Physiol* 130(5):479–496.
3. Cuello LG, et al. (2010) Structural basis for the coupling between activation and inactivation gates in K(+) channels. *Nature* 466(7303):272–275.
4. Cuello LG, Jogini V, Cortes DM, Perozo E (2010) Structural mechanism of C-type inactivation in K(+) channels. *Nature* 466(7303):203–208.
5. Imai S, Osawa M, Takeuchi K, Shimada I (2010) Structural basis underlying the dual gate properties of KcsA. *Proc Natl Acad Sci USA* 107(14):6216–6221.
6. Imai S, et al. (2012) Functional equilibrium of the KcsA structure revealed by NMR. *J Biol Chem* 287(47):39634–39641.
7. Cheng WWL, McCoy JG, Thompson AN, Nichols CG, Nimigean CM (2011) Mechanism for selectivity-inactivation coupling in KcsA potassium channels. *Proc Natl Acad Sci USA* 108(13):5272–5277.
8. Wylie BJ, Bhate MP, McDermott AE (2014) Transmembrane allosteric coupling of the gates in a potassium channel. *Proc Natl Acad Sci USA* 111(1):185–190.
9. Baker KA, Tzitzilonis C, Kwiatkowski W, Choe S, Riek R (2007) Conformational dynamics of the KcsA potassium channel governs gating properties. *Nat Struct Mol Biol* 14(11):1089–1095.
10. Ader C, Pongs O, Becker S, Baldus M (2010) Protein dynamics detected in a membrane-embedded potassium channel using two-dimensional solid-state NMR spectroscopy. *Biochim Biophys Acta* 1798(2):286–290.
11. Ader C, et al. (2008) A structural link between inactivation and block of a K+ channel. *Nat Struct Mol Biol* 15(6):605–612.
12. Bhate MP, McDermott AE (2012) Protonation state of E71 in KcsA and its role for channel collapse and inactivation. *Proc Natl Acad Sci USA* 109(38):15265–15270.
13. Cordero-Morales JF, et al. (2007) Molecular driving forces determining potassium channel slow inactivation. *Nat Struct Mol Biol* 14(11):1062–1069.
14. Ostmeyer J, Chakrapani S, Pan AC, Perozo E, Roux B (2013) Recovery from slow inactivation in K+ channels is controlled by water molecules. *Nature* 501(7465):121–124.
15. Kuo C-C, Chen W-Y, Yang Y-C (2004) Block of tetrodotoxin-resistant Na+ channel pore by multivalent cations: Gating modification and Na+ flow dependence. *J Gen Physiol* 124(1):27–42.
16. Silva J (2014) Voltage gated sodium channels. *Handbook Exp Pharmacol* 221:33–49.
17. Babich O, Matveev V, Harris AL, Shirokov R (2007) Ca2+-dependent inactivation of CaV1.2 channels prevents Gd3+ block: Does Ca2+ block the pore of inactivated channels? *J Gen Physiol* 129(6):477–483.
18. Smith PL, Baukrowitz T, Yellen G (1996) The inward rectification mechanism of the HERG cardiac potassium channel. *Nature* 379(6568):833–836.
19. Shi N, Ye S, Alam A, Chen L, Jiang Y (2006) Atomic structure of a Na+- and K+-conducting channel. *Nature* 440(7083):570–574.
20. Alam A, Jiang Y (2009) High-resolution structure of the open NaK channel. *Nat Struct Mol Biol* 16(1):30–34.
21. Derebe MG, et al. (2011) Tuning the ion selectivity of tetrameric cation channels by changing the number of ion binding sites. *Proc Natl Acad Sci USA* 108(2):598–602.
22. Alam A, Jiang Y (2009) Structural analysis of ion selectivity in the NaK channel. *Nat Struct Mol Biol* 16(1):35–41.
23. Sauer DB, Zeng W, Raghunathan S, Jiang Y (2011) Protein interactions central to stabilizing the K+ channel selectivity filter in a four-sited configuration for selective K+ permeation. *Proc Natl Acad Sci USA* 108(40):16634–16639.
24. Doyle DA, et al. (1998) The structure of the potassium channel: Molecular basis of K+ conduction and selectivity. *Science* 280(5360):69–77.
25. Sauer DB, Zeng W, Canty J, Lam Y, Jiang Y (2013) Sodium and potassium competition in potassium-selective and non-selective channels. *Nat Commun* 4:2721.
26. Heginbotham L, Kolmakova-Partensky L, Miller C (1998) Functional reconstitution of a prokaryotic K+ channel. *J Gen Physiol* 111(6):741–749.
27. Morrison EA, Henzler-Wildman KA (2012) Reconstitution of integral membrane proteins into isotropic bicelles with improved sample stability and expanded lipid composition profile. *Biochim Biophys Acta* 1818(3):814–820.
28. Cornilescu G, Delaglio F, Bax A (1999) Protein backbone angle restraints from searching a database for chemical shift and sequence homology. *J Biomol NMR* 13(3):289–302.
29. Shen Y, Delaglio F, Cornilescu G, Bax A (2009) TALOS+: A hybrid method for predicting protein backbone torsion angles from NMR chemical shifts. *J Biomol NMR* 44(4):213–223.
30. Roux B, et al. (2011) Ion selectivity in channels and transporters. *J Gen Physiol* 137(5):415–426.
31. Furini S, Domene C (2013) K(+) and Na(+) conduction in selective and nonselective ion channels via molecular dynamics simulations. *Biophys J* 105(8):1737–1745.
32. Hodgkin AL, Keynes RD (1955) The potassium permeability of a giant nerve fibre. *J Physiol* 128(1):61–88.
33. Alam A, Jiang Y (2011) Structural studies of ion selectivity in tetrameric cation channels. *J Gen Physiol* 137(5):397–403.
34. Ye S, Li Y, Jiang Y (2010) Novel insights into K+ selectivity from high-resolution structures of an open K+ channel pore. *Nat Struct Mol Biol* 17(8):1019–1023.
35. Manley G, Loria JP (2012) NMR insights into protein allostery. *Arch Biochem Biophys* 519(2):223–231.
36. Ader C, et al. (2009) Coupling of activation and inactivation gate in a K+-channel: Potassium and ligand sensitivity. *EMBO J* 28(18):2825–2834.
37. Solyom Z, et al. (2013) BEST-TROSY experiments for time-efficient sequential resonance assignment of large disordered proteins. *J Biomol NMR* 55(4):311–321.
38. Favier A, Brutscher B (2011) Recovering lost magnetization: Polarization enhancement in biomolecular NMR. *J Biomol NMR* 49(1):9–15.
39. Hyberts SG, Takeuchi K, Wagner G (2010) Poisson-gap sampling and forward maximum entropy reconstruction for enhancing the resolution and sensitivity of protein NMR data. *J Am Chem Soc* 132(7):2145–2147.
40. Hyberts SG, Milbradt AG, Wagner AB, Arthanari H, Wagner G (2012) Application of iterative soft thresholding for fast reconstruction of NMR data non-uniformly sampled with multidimensional Poisson Gap scheduling. *J Biomol NMR* 52(4):315–327.
41. Delaglio F, et al. (1995) NMRPipe: A multidimensional spectral processing system based on UNIX pipes. *J Biomol NMR* 6(3):277–293.
42. Vranken WF, et al. (2005) The CCPN data model for NMR spectroscopy: Development of a software pipeline. *Proteins* 59(4):687–696.
43. Takeuchi K, Ng E, Malia TJ, Wagner G (2007) 1-13C amino acid selective labeling in a 2H15N background for NMR studies of large proteins. *J Biomol NMR* 38(1):89–98.
44. Tollinger M, Skrynnikov NR, Mulder FA, Forman-Kay JD, Kay LE (2001) Slow dynamics in folded and unfolded states of an SH3 domain. *J Am Chem Soc* 123(46):11341–11352.
45. Loria JP, Rance M, Palmer AG (1999) A relaxation-compensated Carr-Purcell-Meiboom-Gill sequence for characterizing chemical exchange by NMR spectroscopy. *J Am Chem Soc* 121(16):2331–2332.
46. DeKoster GT, Delaney KJ, Hall KB (2014) A compare-and-contrast NMR dynamics study of two related RRMs: U1A and SNF. *Biophys J* 107(1):208–219.
47. Chill JH, Louis JM, Miller C, Bax A (2006) NMR study of the tetrameric KcsA potassium channel in detergent micelles. *Protein Sci* 15(4):684–698.
48. Lescop E, Kern T, Brutscher B (2010) Guidelines for the use of band-selective radio-frequency pulses in hetero-nuclear NMR: Example of longitudinal-relaxation-enhanced BEST-type 1H-15N correlation experiments. *J Magn Reson* 203(1):190–198.